International Journal of Solids and Structures 50 (2013) 3406–3417

Contents lists available at SciVerse ScienceDirect

International Journal of Solids and Structures

journal homepage: www.elsevier.com/locate/ijsolstr

Numerical estimation of fracture toughness from indentation-induced circumferential cracking in thin films on ductile substrates

S. Steffensen [a,*], N.D. Madsen [b], H.M. Jensen [a]

[a] Aarhus University, Department of Engineering (ENG), Finlandsgade 22, DK-8200 Aarhus N, Denmark
[b] Interdisciplinary Nanoscience Center (iNANO), Aarhus University, Ny Munkegade, Bldg. 1520, DK-8000 Aarhus C, Denmark

ARTICLE INFO

Article history:
Received 8 January 2013
Received in revised form 31 May 2013
Available online 19 June 2013

Keywords:
Thin hard films
Indentation-induced fracture
FEM
Stress
Stress intensity factor
Energy release rate
Crack channeling
Fracture toughness

ABSTRACT

In this paper, a method to estimate fracture toughness, Γ_f, from the first indenter-induced circumferential crack in a thin film is suggested. The method is based on the stresses in the film and finite element simulations are used to estimate these stresses. The film is taken to be linear elastic while plasticity is included in the substrate. Delamination is not taken into account in the method and the film is perfectly bonded to the substrate. The stress in the film is used to estimate the location where the circumferential crack will initiate from a defect in the film surface. The location is found to be at a distance away from the indenter which correlate with experiments. Also, the stress is used to calculate the stress intensity factor and the energy release rate for a plane strain crack. The energy release rate for the plane strain crack is then used to calculate the energy release for a crack channeling around the indenter forming the circumferential crack. By the energy release rate for the channeling crack fracture toughness is estimated independent of the initial defects in the film provided such defects exist. If the initial defects are smaller than a required minimum value, fracture toughness is overestimated by this method and this overestimation is calculated. Besides fracture toughness, the energy release rate for the channeling crack is used to estimate the depth of the plane strain crack which is found to be smaller than the film thickness.

The method is used to estimate the fracture toughness, Γ_f, for an alumina (Al_2O_3) film using the critical indentation depth. In order to verify the result the estimated crack radius is compared to the actual radius of the circumferential crack in the alumina. The differences between the two radius is found to be within a few percent.

1. Introduction

During the past decades, thin films have been deposited on mechanical components to improve their tribology and mechanical properties. Substrates subjected to contact loading such as cutting tools and bearings are often coated to enhance wear resistance. However, use of thin films are usually accompanied by failure due to brittle fracture. It is a hypothesis that fracture toughness and the crack pattern are linked to the wear resistance of the film and that the parameters governing this pattern can be used to optimize the film. To understand and optimize the wear properties of the film, it is of paramount importance to know the mechanical properties such as the Young's modulus, E, hardness, H, and fracture toughness, Γ_f.

Due to the thickness of thin films, nano-indentation has become a commonly used technique, and procedures for extracting mechanical properties such as hardness and modulus have been established by Oliver and Pharr (1992).

Fracture modes affecting thin films and coatings of various materials have been extensively studied using indentation and general three types of fracture has been observed; Radial cracks that initiate on the median planes, near-contact Hertzian cone fractures and circumferential ring cracks that initiate well outside the contact (An et al., 1996; Chai et al., 1999; Chai and Lawn, 2004; Fischer-Cripps et al., 1996; Lardner et al., 1997; Lee et al., 1998a,b; Lawn et al., 2000; Miranda et al., 2001; Pajares et al., 1996; Swain and Mencik, 1994; and Wuttiphan et al., 1996).

Several experimental studies have shown that formation of radial and circumferential cracks initiating during indentation is traceable as a discontinuity in the indenter response (Hainsworth et al., 1998; Whitehead and Page, 1992; Weppelmann and Swain, 1996).

Besides experiments, numerical analysis have been used to study thin films during indentation in order to understand the stress distribution in the film and the evolution of the plastic zone in the substrate beneath the indenter (Abdul-Baqi and der Giessen, 2002; Bhattacharya and Nix, 1988; Fischer-Cripps et al., 1996;

* Corresponding author. Tel.: +45 4189 3000; fax: +45 4189 3001.
E-mail addresses: sost@iha.dk (S. Steffensen), nisdam@phys.au.dk (N.D. Madsen), hmj@agse.dk (H.M. Jensen).

0020-7683/$ - see front matter © 2013 Elsevier Ltd. All rights reserved.
http://dx.doi.org/10.1016/j.ijsolstr.2013.06.009

Lardner et al., 1997; Lee et al., 1998a; Pachler et al., 2007; Sriram et al., 2003; Vanimisetti and Narasimhan, 2006; and Weppelmann and Swain, 1996).

In order to understand the mechanics of the crack propagations in the film during indentation, numerical simulations have been used to calculate the energy release rate, G, and the stress intensity factor, K, for a crack running through the film (Abdul-Baqi and der Giessen, 2002; Chai et al., 1999; Chai and Lawn, 2004; Miranda et al., 2001; Sriram et al., 2003; Vanimisetti and Narasimhan, 2006, 2007; Weppelmann and Swain, 1996).

Also, methods to calculate fracture toughness, Γ_f, for the film during indentation, bending, and micro-tensile testing have been suggested, and, recently, Zhang and Zhang (2012) have summarized most of these methods. The suggested methods for circumferential cracks have all been based on different methods to estimate the consumed energy from the discontinuity in the indenter response and common for all of the methods are that it is assumed that the crack in the film runs all the way to the interface when it is initiated.

Li et al. (1997) and Li and Bhushan (1998) suggested that the critical energy release rate for the film, i.e. fracture toughness can be estimated as

$$\Gamma_f = \frac{U}{\pi \cdot D_{crack} \cdot t_f} \tag{1}$$

where D_{crack} is the diameter of the circumferential crack, t_f is the thickness of the film and U is the fracture energy. They assumed that the crack is dominated by mode I fracture and that the crack runs instantaneously all the way to the interface between the film and the substrate. The fracture energy, U, was suggested to be the irreversible work of the indenter during fracture and they proposed that it is given by the area between an extrapolated loading curve and the discontinuity in the original loading curve, i.e. the area given by the three points *ABC* in Fig. 1.

Later, Toonder et al. (2002) suggested a method to estimate a lower and upper bound for the irreversible work for both load and displacement controlled indentations. For the load controlled case, the lower and upper bounds for the work are shown in Fig. 1 as the area given by the points *OAC* and *ACFG*, respectively.

Michel et al. (2006) realized that a part of the consumed energy, U, estimated from the discontinuity in the indenter response was due to plastic deformation in the substrate and proposed another method. They suggested that the area given by the points *ACH* i Fig. 1 represent the energy release during fracture and the area given by the points *CFGH* represent the energy of substrate deformation. The point H, given by the segment OC, represent the loading curve of the substrate.

Chen and Bull (2009) used a method by Cheng et al. (2002) to obtain the unloading curve *AJ* and *CI*, and used those to estimate the consumed energy, U. They argued that the lower and upper boundary for the consumed energy, U, was given by the area between the points *ACJ* and *ACFJ* in Fig. 1, respectively and considered the area *ACIJ* as representing the fracture energy, U. The method by Cheng et al. (2002) to obtain the unloading curve was developed for a bulk material and without fracture.

In this paper, we suggest a new method for estimating fracture toughness, Γ_f, based on the first indenter-induced circumferential crack in a thin brittle film, without estimating the irreversible work of the indenter during fracture. The method is based on the stress in an uncracked thin film, and it is independent of the length of the initial defects in the film, a_{init}, and the depth of the crack when the crack stops propagate, a_{max}. Numerical analyses of a conical indentation in a thin brittle film perfectly bonded to a ductile substrate are performed in order to obtain the stresses in the film. Based on the stresses in the film, closed form expressions are used to calculate fracture toughness. Besides fracture toughness, the method give the length of the crack to which unstable crack propagation stops, a_{max}, and informations about the length of the required initial defects in the film, a_{init}, for the method to be accurate.

Wang et al. (1998) used a similar method for calculating the fracture toughness, Γ_f, for circumferential cracks in the indentation crater. They found that the stress gradients in the film caused by bending can be neglected whenever the cracks propagates fully through the film and did not investigate the case where the cracks only propagate partially through the film. Also, they did not investigate circumferential cracks located outside the indenter crater as seen in experiments.

2. Fracture behavior

Fig. 2 shows a circumferential crack in a Al_2O_3 film with thickness 1.2 μm, taken with a scanning electron microscope (SEM). The circumferential crack and the permanent deformation from the indenter is seen in the picture. The reversible energy in the system during indentation is not large due to plasticity in the substrate. Thus, it is obvious from Fig. 2 that the circumferential crack has not been formed beneath the indenter or at the edge of contact. Also, it is seen that no cracks have initiated prior to the circumferential crack.

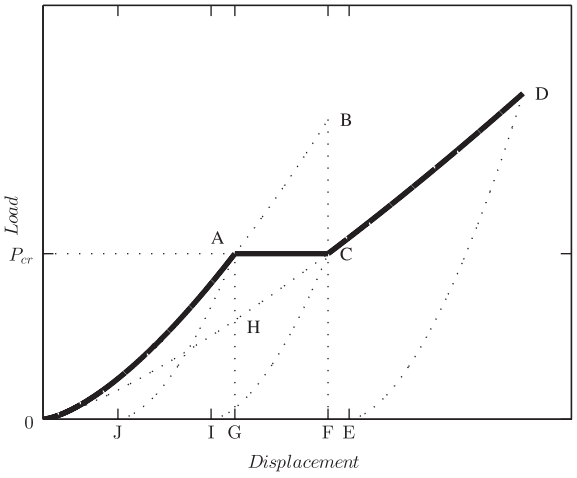

Fig. 1. Schematic diagram representing the fracture energy U of a coating at the discontinuity in the indenter response.

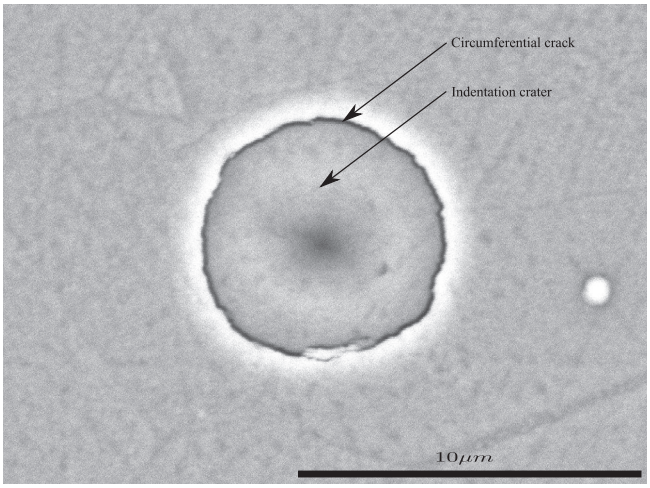

Fig. 2. Indenter-induced circumferential crack in an Al_2O_3 film.

For crack propagation to occur, the critical energy release rate of the material, the fracture toughness, Γ_f, must be reached. The energy release rate for a plane strain crack, G_{ps}, under mode *I*, *II* and *III* loading is related to the stress intensity factors K_I, K_{II} and K_{III} assuming small scale yielding in the film. The mode *I* stress intensity factor, K_I, is an opening mode that arise due to tensile stress perpendicular to the crack, σ_{rr}, the mode *II* stress intensity factor, K_{II}, is a sliding mode that arise due to in-plane shear stress, σ_{rz}, and the mode *III* stress intensity factor, K_{III}, is a tearing mode that arise due to anti-plane shear stress, $\sigma_{r\theta}$. Due to axisymmetry the mode *III* stress intensity factor, K_{III}, does not contribute to the energy release rate for the plane strain crack, G_{ps} ($\sigma_{r\theta} = 0$ for circumferential cracks, see Section 3). Thus, the relationship between the energy release rate for a plane strain crack, G_{ps}, and the stress intensity factors, *K*, for mode *I* and *II* is given by

$$G_{ps} = K_I^2\left(\frac{1-\nu^2}{E}\right) + K_{II}^2\left(\frac{1-\nu^2}{E}\right) \tag{2}$$

where *E* is Young's modulus and ν is Poisson's ratio.

The energy release rate for the plane strain crack, G_{ps}, is based on tensile radial stress, σ_{rr}, and in-plane shear stress, σ_{rz}, and numerical simulations are used to investigate the stress distribution in the film.

In this study it is assumed that the circumferential crack will propagate perpendicular to the surface at all indentation depths, δ_i, see Fig. 3. Complexities in the microstructure of the film such as grain structure may influence the direction of the crack propagation. In this paper the grain structure is ignored and only circumferential cracks in homogeneous films are investigated.

3. Numerical simulations

In this work, the general-purpose finite element code MSC.Marc is used to analyze the contact problem of indentation in a film-substrate system. The objective for the numerical simulation is to investigate the stress distribution in the film at distances greater than the contact radius, R_i. A large deformation and large strain nonlinear procedure (Updated Lagrangian) is used to capture the nonlinear effect that arise due to large deformations, contact and plasticity. Conventional plasticity theory has been applied and no significant differences between kinematic and isotropic hardening theories have been observed.

Circumferential cracks are usually induced by axisymmetric indenters and in this study, a conical indenter with a half angle at 70.3° is used. Also, the conical indenter is assumed frictionless, rigid and with a 0.76 μm tip rounding.

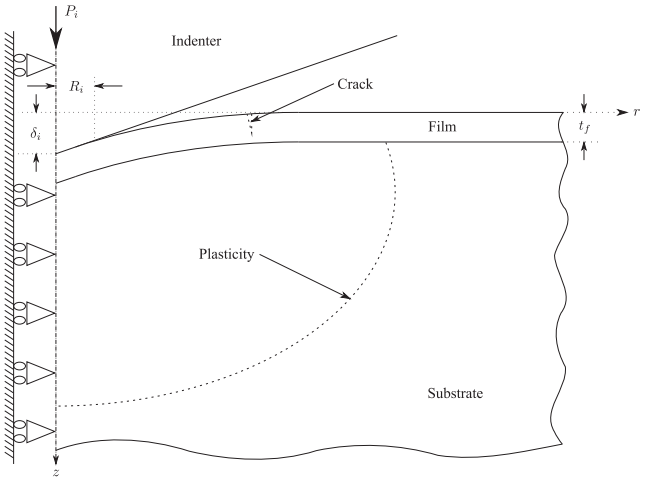

Fig. 3. Illustration of geometry used for the finite element simulations and illustration of the plastic zone in the substrate.

An illustration of the model used for the analysis is shown in Fig. 3. It shows an axisymmetric section of a film of thickness t_f, bonded to a substrate during indentation where P_i is the indenter load, δ_i is the indentation depth and R_i is the contact radius.

The constitutive model used for the elastic–plastic substrate requires input in form of an uni-axial stress–strain curve to describe the nonlinear part. The film is assumed linear elastic, isotropic, free of defects and without residual stresses. Residual stresses can be included but the influence is not investigated in this paper. The substrate is elastic–plastic, isotropic, without defects and free of residual stresses. Delamination is not investigated in this paper so perfect adhesion between film and substrate is assumed.

The elements used in the mesh are four-node, isoparametric, arbitrary quadrilaterals for axisymmetric applications. When geometry, load and boundary conditions are all axisymmetric, nothing varies in the θ direction and material points have only displacement in the radial *r* and axial *z* direction. Thus, the element output of strain is

$$\boldsymbol{\epsilon} = \begin{bmatrix} \epsilon_{rr} & \epsilon_{rz} & 0 \\ \epsilon_{rz} & \epsilon_{zz} & 0 \\ 0 & 0 & \epsilon_{\theta\theta} \end{bmatrix} \tag{3}$$

The elements used in the mesh are gradually refined towards the indenter in order to represent the stress concentrations in the area near the indenter. To ensure that the results are not affected by the size of the elements, convergence studies are performed.

Also, a sensitivity study of the size of the model was performed to avoid effects from the boundary far away from the indenter zone and the model is chosen such that these effect will not influence the stress distribution in the film near the indenter.

The focus of the discussion in this paper is on introducing a method to estimate fracture toughness of thin films, Γ_f, based on observing when the first circumferential crack propagate, and not how material and geometric parameters influence the fracture toughness. Later, a paper will follow that focus on parameters influence on the fracture toughness. Thus, only one set of material properties have been used and the choice of parameters are made to match experimental results for an alumina thin film on stainless steel. The elastic material properties used to explain the method are $E_f = 235$ GPa, $\nu_f = 0.3$ and $E_s = 210$ GPa, $\nu_s = 0.3$ for film and substrate respectively, where *E* corresponds to the elastic modulus and ν to Poisson's ratio. The nonlinear material properties for the substrate are given by an uni-axial stress–strain curve for stainless steel 316 (X5CrNiMo18-10) at 20 °C shown in Fig. 4 (Doege et al., 1986). The stress–strain response is only given for the nonlinear part. In Fig. 3, the importance of plasticity in the substrate is illustrated by the size of the plastic zone in the substrate compared to the film thickness, t_f, and the location of the fracture for a given indentation depth, δ_i/t_f.

Sometimes, an adhesion layer is added between the substrate and the film in order to reduce delamination. The method to estimate fracture toughness for the film, Γ_f, is independent of the adhesion layer. Preliminary studies indicates that the adhesion layer can be neglected if the thickness of the adhesion layer, t_b, is small compared to the film thickness, t_f, and if fracture occur early in the indentation process ($\delta_i/t_f \lessapprox 1$). However, this is a subject for further studies.

If the adhesion layer is significant, it has to be included in the numerical model but the procedure for estimating fracture toughness for the film, Γ_f, is the same. Due to the focus in this paper the adhesion layer is neglected and is assumed throughout the rest of the paper. The film thickness $t_f = 1.2$ μm.

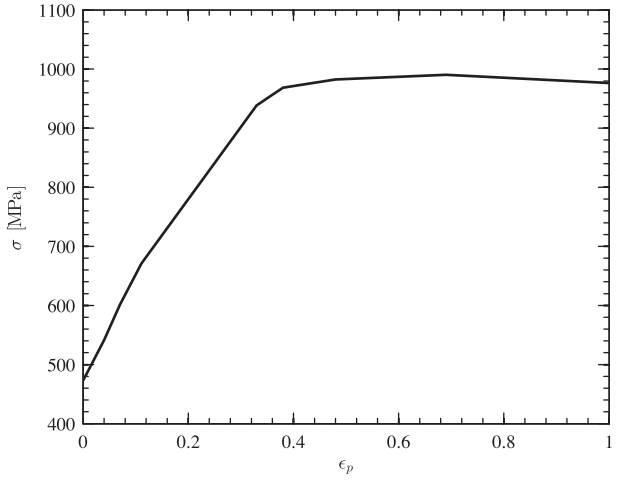

Fig. 4. Nonlinear part of the stress–strain response for stainless steel at 20 °C used as substrate used in the numerical model.

The material parameters are chosen to correspond to the setup used in the experiments, see Section 12.

4. Stress distribution in the film

Results from the numerical simulations are used to investigate whether the circumferential crack will propagate from the film surface or the interface and to find the radius of the crack path, r_{crack}. Also, the stress will later be used to estimate fracture toughness for the film, Γ_f. The stress components driving the circumferential cracks are the radial stress, σ_{rr}, and the in-plane shear stress, σ_{rz}, as described in Section (2). The possibility of crack propagation beneath the indenter is ignored because only circumferential cracks at distances greater than the contact radius, R_i, are observed during the experiments.

Fig. 5(a) shows the radial stress, σ_{rr}, in the film at the surface plotted against the ratio r/R_i for various indentation depths, δ_i/t_f. The radial stress is tensile at the surface with a peak located outside the contact zone for all indentation depths, δ_i/t_f.

The tensile radial stress, σ_{rr}, will open the crack and contribute to the mode I stress intensity factor, K_I. If the crack is to propagate from the film surface primarily by mode I loading, the crack will most likely propagate from a crack-like defect located where the radial stress peaks, assuming there is a high density of defects in the film and the defects are of the same size and evenly distributed in the film.

Fig. 5(b) shows the radial stress, σ_{rr}, in the film at the interface plotted against the ratio r/R_i for various indentation depths, δ_i/t_f. The radial stress is tensile near the contact zone and compressive at distances away from the indenter with a peak in the compressive radial stress at the same distance, r/R_i, as the tensile radial stress peaks in Fig. 5(a). The tensile radial peak stress in Fig. 5 and the compressive radial peak stress in Fig. 5(b) at the same distance, r/R_i, indicates that the radial stress distribution through the film at that distance is primarily due to bending in the film.

The circumferential cracks detected during experiments are discovered at a distance away from the indenter and not beneath the indenter. Cracks may have propagated from the interface beneath the indenter but in that case they have not reached the surface since they have not been observed in the present systems during experiments. Thus, these cracks are not investigated in this paper. Cracks propagating from the interface have been observed in other systems by Chai et al. (1999); Lawn et al. (2000) and Chai and Lawn (2004).

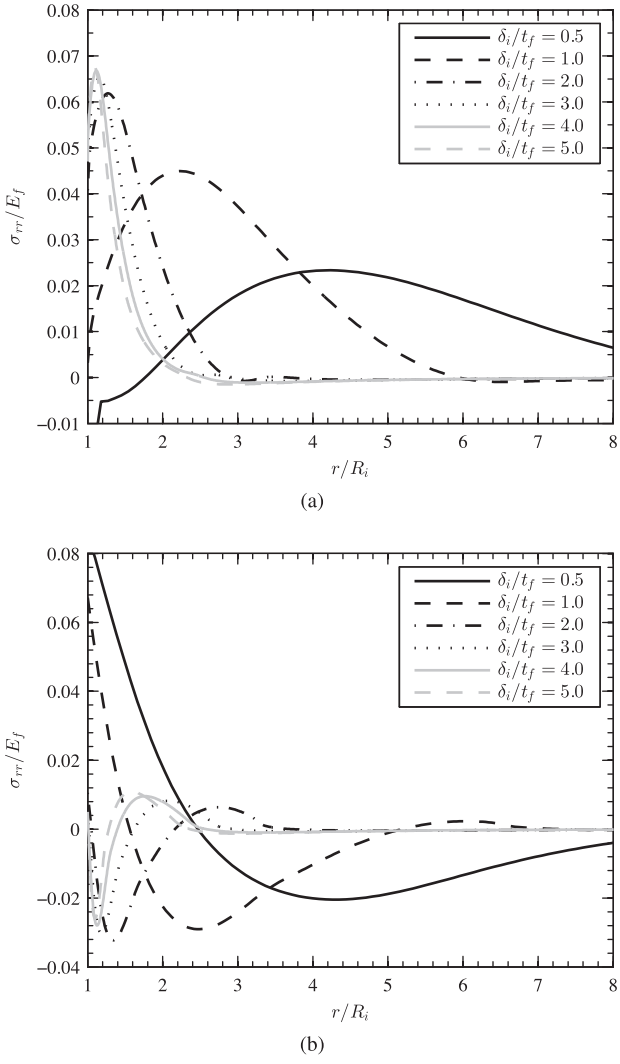

Fig. 5. Radial stress in the film for various indentation depths at: (a) the surface and (b) the film/substrate interface.

The compressive radial stress, σ_{rr}, in the film at the interface will close the crack tip and stop the crack propagating from the surface. This will prevent the crack from propagating all the way to the interface.

In Fig. 5(a) it might seems like the radial stress, σ_{rr}, peak is moving closer to the indenter with deeper indentation, δ_i/t_f, but that is not the case as the indentation radius, R_i, also increases. In Fig. 6, the radial stress at the surface is plotted against the ratio $(r - R_i)/t_f$, i.e. the distance from the indenter contact instead of the axis of symmetry It can be seen that the radial stress peak is located more than a film thickness, t_f, away from the contact radius for all indentation depths, δ_i.

The second type of stress that contributes to the crack propagation of the circumferential cracks is the in-plane shear stress, σ_{rz}. The in-plane shear stress has shown to be parabolic through the film and reach a peak at the middle of the film as known from plate theory (Timoshenko and Woinowsky-Krieger, 1959). Also, the shear stress is zero at the free surface but it is also found to be approximately zero at the interface. Thus, the shear stress will not have a large influence on the initial propagation of the crack. When the crack is propagating towards the middle of the film the shear stress is increasing and this may lead to mixed mode loading conditions. Also, the mixed mode loading conditions may affect the direction of the crack propagation. In Fig. 7 the normal-

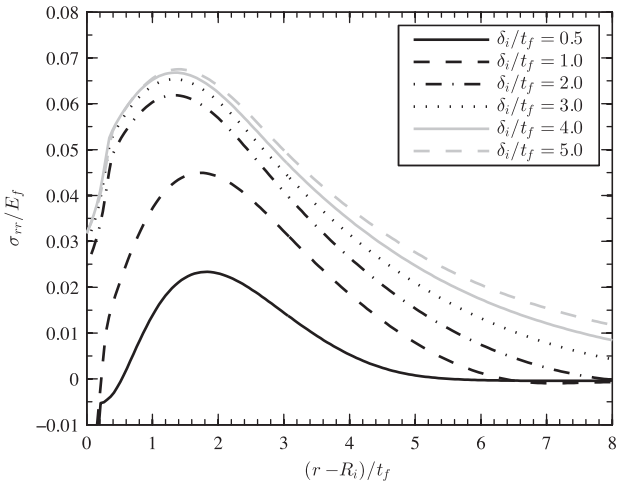

Fig. 6. Radial stress in the film at the surface for various indentation depths.

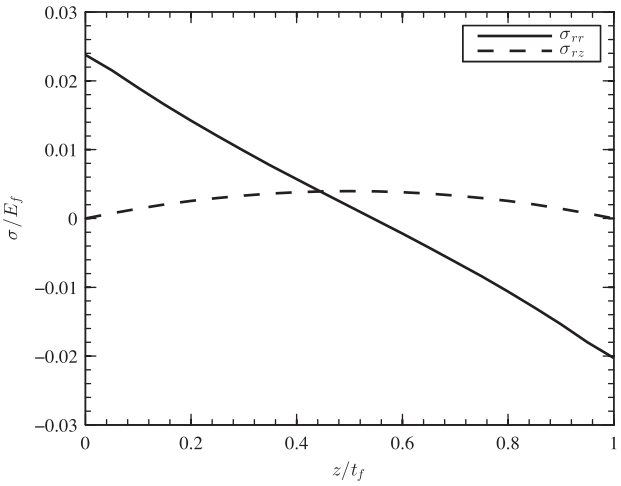

Fig. 8. Radial and shear stress through the film for the indentation depth $\delta_i/t_f = 0.5$ at the location of peak radial stress at the surface, $r/t_f = 2.3$.

ized in-plane shear stress at the distance away from the indenter where the radial stress at the surface peaks, σ_{rz}, is plotted against the indentation depth, δ_i/t_f.

The in-plane shear stress, σ_{rz}, in the film is in general smaller than the radial stress at the surface, σ_{rr}, and for that reason, crack location will most likely be dominated by the radial stress, mode *I* loading, when the crack is initiating from the surface or the interface. When the crack has initiated, the in-plane shear stress may be more dominating and for that reason, the radial stress and the in-plane shear stress through the film is investigated at the location where the radial stress at the surface peaks. Fig. 8 shows the radial stress and the in-plane shear stress plotted against the ratio z/t_f, i.e. the distance through the film, for indentation depth, $\delta/t_f = 0.5$.

The radial stress and the shear stress through the film is behaving as the plate theory describes (Timoshenko and Woinowsky-Krieger, 1959). The magnitude of the in-plane shear stress, σ_{rz}, compared to the radial stress, σ_{rr}, is of a size where it can be neglected without adding a significant error to the calculation of fracture toughness, Γ_f, which it is done in this study. This means that the circumferential crack perpendicular to the surface is entirely dominated by mode *I* loading, i.e. the last term of Eq. (2) is neglected. Though, the in-plane shear stress may become significant when the crack is approacing the interface and an intensive investigation of this has been conducted by Steffensen and Jensen (2013).

Also, Fig. 8 shows that the radial stress, σ_{rr}, through the film is primarily due to radial bending stresses, σ_{rr}^b, and that membrane stresses, σ_{rr}^m, are insignificant for the indentation depth $\delta_i/t_f = 0.5$. This is due to the approximate linear distribution of the radial stress through the film and that the radial stress is approximately zero half way through the film. The membrane stress is taken as the radial stress in the middle of the film, and the bending stress as the radial stress at the surface with the membrane stress subtracted. In Fig. 5 the tensile radial stress peaks at the surface and the compressive radial stress peaks at the interface both seems to continue to increase with indentation depth, δ_i. In Fig. 9, the bending stress and membrane stress are plotted against the indentation depth, δ_i/t_f. It can be seen that the bending stress is increasing until it reaches a constant value at the indentation depth, $\delta_i/t_f \approx 2$. The membrane stress is compressive in the beginning but increases and becomes tensile shortly after. At the indentation depth, $\delta_i/t_f \approx 1.5$, the increase levels off. The membrane stress is never large enough to make the radial stress at the interface tensile and at all times during indentation, the bending stress is dominating.

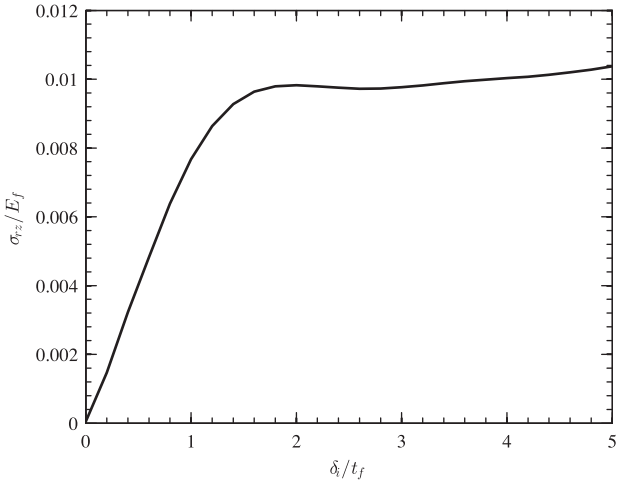

Fig. 7. In-plane shear stress in the middle of the film during indentation at the location of peak radial stress at the surface.

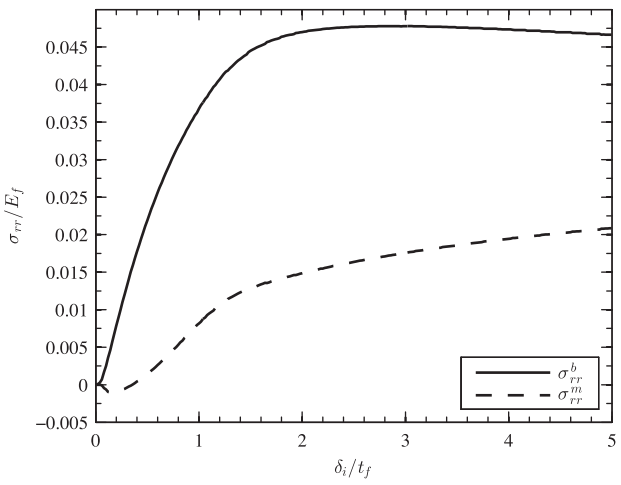

Fig. 9. Bending stress and membrane stress in the film during indentation at the location of peak radial stress at the surface.

5. Stress intensity factor

In order to gain a greater understanding of the circumferential cracks, the stress intensity factor, K, is evaluated through the film based on the radial stresses, σ_{rr}, from the numerical simulation. Unfortunately, the radial stress through the film does not scale with the indentation depth, δ_i, meaning that the stress intensity factor cannot be scaled either. As a result, the stress intensity factor has to be calculated for each depth of indentation. Due to computation time, closed form expressions are used instead of numerical methods to calculate the stress intensity factor.

In Section 2 it was explained why the tearing mode, K_{III}, is ignored and in Section 4 the arguments for neglecting the sliding mode, K_{II}, was discussed. Thus, only the opening mode, K_I, is studied in this section.

For linear elastic materials, superposition applies. Thus, the radial stress, σ_{rr}, in an uncracked film can be used to calculate the stress intensity factor, K, for a circumferential crack in the film. For calculation of the stress intensity factor, closed form expressions for an edge crack in a semi-infinite plane are used (Tada et al., 2000).

The geometry of a circumferential crack in a thin film is different from the geometry of a one-dimensional crack in a semi-infinite plane and this will give rise to an error. This error vanishes as the ratio of the film thickness and the radius of the crack location, t_f/r_{crack}, tends to zero. Also, the interface between the film and the substrate complicates the calculation due to the elastic mismatch between the film and the substrate, E_f/E_s, and plasticity in the substrate. The closed form expressions does not take these effect into account but it is assumed that the error introduced is negligible until the crack tip is approaching the interface, i.e. the error $\to 0$ as $a/t_f \to 0$. These effects have been studied using numerical methods by Steffensen and Jensen (2013) and a good agreement with the closed form linear fracture mechanics expressions by Tada et al. (2000) was found up to a crack length of $a/t_f \approx 0.9$. The errors are approximately below 8% even at $\delta_i/t_f = 0.25$. Results based upon the two approaches will be shown in Fig. 14.

Superposition applies to the stress intensity factors, K, since it depends linearly on the stresses. Thus, the stress intensity factor, K, can be divided into two parts, one caused by a constant stress acting on the crack and one caused by a stress linearly decreasing along the length of the crack, a. Fig. 10 illustrates how the stress acting on the crack is divided into a constant and a linearly varying stress.

The stress intensity factor, K, of a plane strain crack caused by the constant stress is calculated using a closed form expression for an edge crack in a semi-infinite plane (Tada et al., 2000)

$$K_I = \sigma \cdot \sqrt{\pi \cdot a} \cdot \frac{2}{\pi} \cdot \sin^{-1}\left(\frac{b}{a}\right) \cdot F\left(\frac{b}{a}\right) \tag{4}$$

where σ is the stress, a is the length of the crack, b is length of the crack where the stress is applied and $F(b/a)$ is a geometric constant

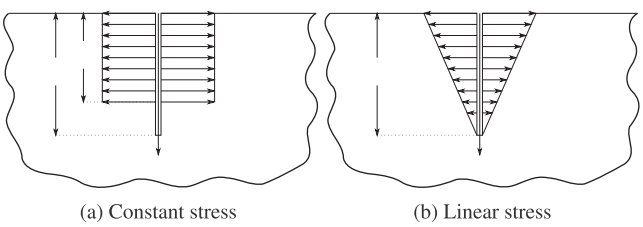

Fig. 10. Illustration of the stress applied on the crack used in the superposition.

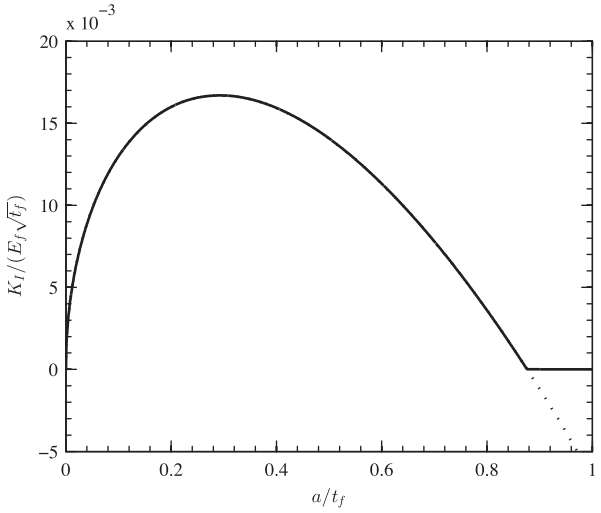

Fig. 11. Stress intensity factor for a crack propagating through the film for indentation depth $\delta_i/t_f = 0.5$ and at the location of peak radial stress at the surface, $r/t_f = 2.3$.

given by $F(b/a) = 1.3 - 0.18 \cdot b/a$. When calculating the stress intensity factor for the circumferential crack $a = b$ at all time.

The stress intensity factor, K, of a plane strain crack caused by the linearly varying stress is calculated using a closed form expression for an edge crack in a semi-infinite plane (Tada et al., 2000)

$$K_I = 0.439 \cdot p \cdot \sqrt{\pi \cdot a} \tag{5}$$

where a is the length of the crack and p is given by the stress distribution along the crack $\sigma(z) = p(1 - z/a)$. Then, the two stress intensity factors are added in order to calculate the total mode I stress intensity factor.

Fig. 11 shows the stress intensity factor for a plane strain crack, K, propagating through the film for indentation depth $\delta_i/t_f = 0.5$. When the crack starts propagating from the surface the stress intensity factor increases until it reaches a peak at a crack length $a/t_f \approx 0.3$. Then, it starts decreasing and at the length of the crack $a/t_f \approx 0.85$ it reaches zero. The dashed line shows that the solution is negative when the length of the crack is longer than $a/t_f \approx 0.85$ meaning that the compressive radial stress, σ_{rr}, near the interface have closed the crack tip. Consequently, the crack propagation will stop before it reaches the interface due to the closing crack tip and lack of in-plane shear stress, σ_{rz}, i.e. mode II loading.

6. Energy release rate

Using Eq. (2) the energy release rate for a plane strain crack, G_{ps}, can be calculated once the stress intensity factor, K, has been calculated. In Fig. 12 the energy release rate, G_{ps}, is plotted against the length of the crack, a/t_f, for the indentation depth $\delta_i/t_f = 0.5$.

It is possible to estimate the fracture toughness, Γ_f, on the basis of the energy release rate for a plane strain crack, G_{ps}, through the film if the length of the initial defects in the film is known. The fracture toughness is simply read of the energy release rate curve associated with the indentation depth, δ_i/t_i, at the known length of the initial defect, a_{init}/t_f.

Informations about the initial defects in the film are in general not available due to the complexity of measuring the length of the defect. For that reason is it complicated to estimate fracture toughness, Γ_f, this way and an alternative more robust method is devised in Section 7.

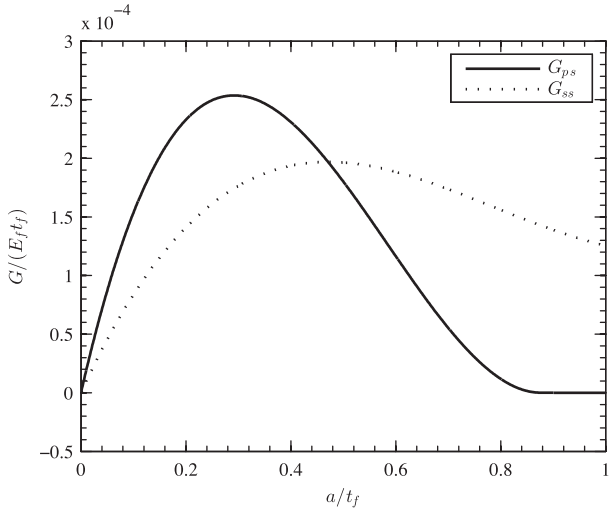

Fig. 12. Energy release rate of the plane strain crack G_{ps} propagating through the film and energy release rate of the channel front G_{ss} for indentation depth $\delta_i/t_f = 0.5$ and at the location of peak radial stress at the surface, $r/t_f = 2.3$.

7. Crack channeling

Until now we have been focusing on a plane strain edge crack propagating towards the interface. When the plane strain crack is nucleated from an initial crack-like defect it may activate a channel crack that runs around the indenter forming the circumferential crack, i.e. a crack out of the plane. A crack channeling through a film is shown in Fig. 13. By Fig. 12 it may become more energetically favorable for the crack to propagate by channeling instead of continued propagation of the plane strain crack due to the decrease in energy release rate for the plane strain crack, G_{ps}.

When the crack is channeling, the front of the channel self-adjust to a curved shape such that the energy release rate for the plane strain crack, G_{ps}, at each instant of growth is the same at every point. The energy release rate for the channeling, G_{ss}, will approach a steady-state value after it has propagated a few times the film thickness, t_f. When the channel crack propagates, the front maintains its shape and the energy release rate no longer depends on the channeling length, or the initial defect geometry. In the wake of the channeling crack, the cross-section profile of the plane strain crack will retain its shape and the shape of the channeling front does not influence the calculation of the energy release rate for the channeling (Hutchinson and Suo, 1991). The energy release rate for the channel is evaluated using (Beuth, 1992)

$$G_{ss}(a) = \frac{1}{a}\int_0^a G_{ps}(\tilde{a})d\tilde{a} \tag{6}$$

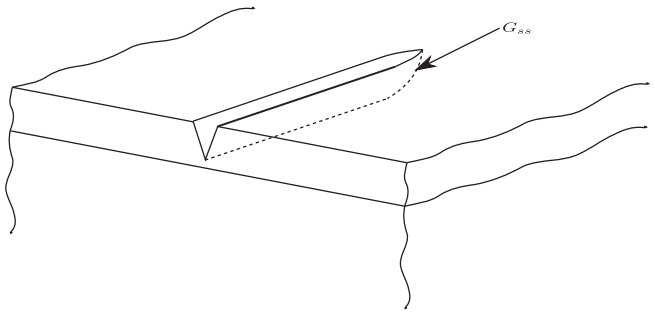

Fig. 13. Illustration of a channel crack propagating through the film.

where G_{ps} is the energy release rate of a plane strain crack and a is the depth of the crack.

Eq. (6) is valid for steady-state channeling which is accurate if the radius of the crack, r_{crack}, is large compared to the film thickness, t_f. Due to the geometry of the indenter, the radial stress, σ_{rr}, is symmetric all the way around the indenter but due to of the curvature of the crack, κ, it is not fully steady-state. When the curvature, κ, is small compared to the film thickness, t_f, is it assumed that the error due to steady-state is small and the error can be neglected.

In Fig. 12, the energy release rate of the plane strain crack, G_{ps}, and the energy release rate of the channel front, G_{ss}, are plotted against the depth of the crack a/t_f for indentation depth, $\delta_i/t_f = 0.5$.

The curve for the energy release rate of the channel front, G_{ss}, peaks where it intersects the curve for the energy release rate of the plane strain crack, G_{ps}. The maximum of the energy release rate of the channel front curve is located by taking the derivative of Eq. (6) with respect to the depth of the crack, a,

$$\frac{dG_{ss}}{da} = \frac{1}{a}G_{ps} - \frac{1}{a^2}\int_0^a G_{ps}(a)da = \frac{1}{a}(G_{ps} - G_{ss}) \tag{7}$$

Thus, when $dG_{ss}/da = 0, G_{ss} = G_{pl}$ defines that the maximum of the curve for the energy release rate of the channel front is located when it intersect the curve for the energy release rate for the plane strain crack (Beuth, 1992).

Also, Fig. 12 delineates the likelihood for which type of crack that will propagate. If the fracture toughness, Γ_f, is above the maximum of the curve for the energy release rate of the plane strain crack, G_{ps}, no cracks will be present and this is independent of the size of the initial defect in the film, a_{init}. If the fracture toughness is between the maximum of the curve for the energy release rate of the plane strain crack and the maximum of the curve for the energy release rate of the channeling front, G_{ss}, a plane strain crack will propagate towards the interface but channeling will not occur. Naturally, the plane strain crack propagation is dependent on the size of the initial defect in the film, a_{init}. If a plane strain crack is initiated it will continue to propagate until the energy release rate for the plane strain crack drops below the fracture toughness. If the fracture toughness is below the maximum of the curve for the energy release rate of the channeling front both types of cracking may occur. Channeling is of course dependent on a plane strain crack being initiated but it is assumed that plane strain cracks initiates all the time during indentation due to a high concentration of defects in the film.

When a channeling crack is initiated, it will propagate through the entire film or until a boundary is reached. During indentation this means that the channel crack will run until it forms a fully circumferential crack or if the channel crack is initiated from more than one plane strain crack, until the channel cracks merge together.

8. Fracture toughness

It is assumed that plane strain cracks do not leave traceable marks in the indenter response, and that a circumferential crack shows up as a discontinuity. Thus, during indentation when fracture is detected, the fracture toughness, Γ_f, can be estimated either from indentation depth, δ_i, indentation load P_i or the radius of the crack, r_{crack}.

Since the channel crack propagates as soon as $G_{ss}(a) = \Gamma_f$, it can be used to calculate fracture toughness without the need for knowing the length of the initial defects, a_{init}, provided these initial defects exceeds a minimum value which will be calculated in Section 11. The error associated with insufficient flaw size will also

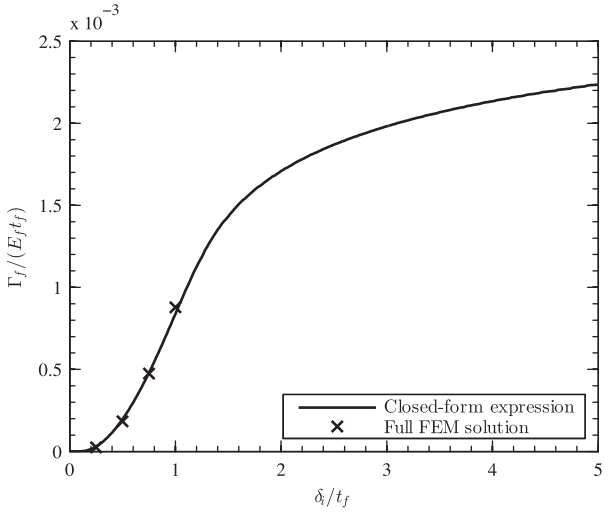

Fig. 14. Fracture toughness of circumferential cracks as a function of critical indentation depth, δ_i/t_f, for unset of a channel crack. Results from Steffensen and Jensen, 2013 based on full FEM formulation are included in the figure.

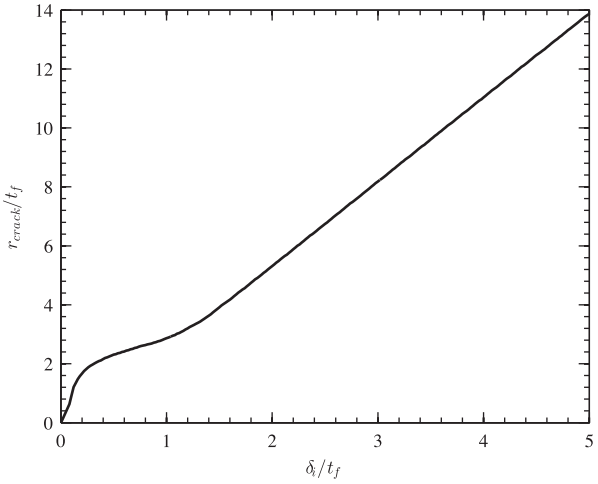

Fig. 15. Radius of circumferential cracks as a function of critical indentation depth, δ_i/t_f, for unset of a channel crack.

be calculated in Section 11. The fracture toughness is given by the peak of the curve for the energy release rate for the channel front, G_{ss}, or the intersection of the two curves for the energy release rate, G_{ps} and G_{ss}. In Fig. 14, the normalised fracture toughness, is plotted as a function of critical indentation depth, δ_i/t_f, for unset of a channel crack which is unique for a given system.

The curve of fracture toughness rapidly increases with indentation depth and at an indentation depth of $\delta_i/t_f \approx 1.5$ it slowly levels off as seen in Fig. 14.

Curves for the fracture toughness as a function of critical indentation load, P_i, or crack radius, r_{crack}, are available from the numerical model but not presented in this paper. Also, if indentation data is not available or if fracture is not traceable in the indentation response, is it possible to estimate fracture toughness on the basis of only the circumferential crack radius, r_{crack}.

9. Crack radius

Besides that the fracture toughness, Γ_f, can be estimated using the crack radius, $r_{,crack}$, the crack radius can be used to verify the estimated fracture toughness. If the crack radius is know from a SEM image it has to be consistent with the crack radius estimated using the simulation. For the two radii to be equal it is of paramount importance that the indenter response from the simulation matches the indenter response from the experiments. Any deviation in the indentation response will cause a deviation between the two radii and the estimated fracture toughness.

In Fig. 15, the crack radius, r_{crack}/t_f, is plotted against the indentation depth, δ_i/t_f. It is seen that the crack radius varies linearly with indentation for indentation depths, $\delta_i/t_f > 1$. For smaller indentations depths, $\delta_i/t_f < 1$, the crack radius shows a nonlinear behavior where it increases rapidly in the beginning of the indentation and then levels off.

10. Crack depth

Besides the fracture toughness, Γ_f, and the circumferential crack radius, r_{crack}, the present method gives information about the maximum depth of the crack during channeling, a_{max}. This information can be used to investigate whether the unstable crack propagation stops before or at the interface. Here, unstable crack propagation refers to cases where the crack channel criterion is exceeded. If the crack propagates all the way to the interface it might lead to complications such as substrate penetration and interface debond. Furthermore, all previous studies assume that the crack propagates fully through the film which may lead to significant errors.

When channeling is initiated, the maximum depth of the crack at the present indentation depth can be estimated by the intersection of the energy release rate for the plane strain crack, G_{ps}, and the energy release rate for the channeling crack, G_{ss}, i.e. $G_{ps}(a) = G_{ss}(a)$ where $a = a_{max}$ due to Eq. (7). Once a channel crack has propagated circumferentially, further crack growth towards the interface requires increased indentation load. In Fig. 16, the maximum depth of the crack during channeling, a_{max}/t_f, is plotted versus the indentation depth, δ_i/t_f. The maximum depth of the crack increases rapidly in the beginning of the indentation. Then, it slowly approaches a constant value, $a_{max}/t_f \approx 0.65$. Thus, at no stage during indentation, the circumferential crack propagate all the way to the interface, in contrast to what is assumed in previous studies by Zhang and Zhang (2012); Li et al. (1997); Li and Bhushan (1998); Toonder et al. (2002); Michel et al. (2006); Chen and Bull (2009) and Wang et al. (1998). Also, that unstable crack propagation can stop before the interface is consistent with experiments by Chai et al. (1999). Their experiment shows a circumferential

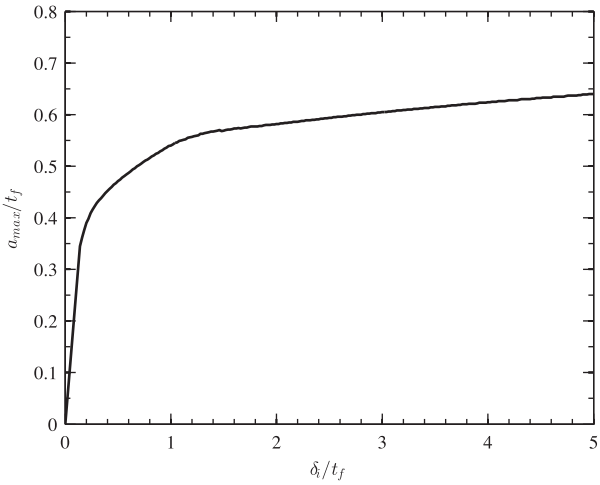

Fig. 16. Crack depth for unstable growth of circumferential cracks as a function of critical indentation depth, δ_i/t_f, for unset of a channel crack.

crack located well outside the contact that has initiated perpendicular to the surface and subsequently deflects horizontally at approximately a quarter layer thickness from the interface.

In Section 5 it was discussed that the elastic mismatch between the film and the substrate, E_f/E_s, and plasticity in the substrate could cause an error in the calculation of the stress intensity factor, K, but it was assumed that the error is neglectable until the crack tip approaches the interface. By the results in Fig. 16, the stress intensity factor near the interface is of minor importance for estimating the fracture toughness since the crack stops far from the interface.

11. Initial defect

Informations about the initial defects gained from the present method are sparse. However, the minimal length of the initial defects, a_{init}, for fracture to initiate at a specific indentation depth, δ_i, can be calculated. This tells us whether the estimated fracture toughness, Γ_f, is accurate or overestimated.

The initial defects will propagate if the energy release rate for the plane strain crack, G_{ps}, is larger than the fracture toughness, i.e. $G_{ps}(a_{init}) > \Gamma_f$. Then, if the fracture toughness is known, a minimum length of the initial defects can be calculated as illustrated in Fig. 17 by the point where the energy release rate for a plane strain crack, G_{ps}, at indentation depth $\delta_i/t_f = 1$ intersects the curve for fracture toughness, Γ_f.

If the length of the initial defects are larger than those required, the initial defects will initiate at a lower indentation depth, $\delta_i/t_f < 1$, as illustrated in Fig. 17 by the point where the energy release rate for a plane strain crack, G_{ps}, at indentation depth $\delta_i/t_f < 1$ intersects the curve for the fracture toughness, Γ_f. The plane strain crack will then propagate until the energy release rate for the plane strain crack, G_{ps}, is lower than fracture toughness, Γ_f, i.e. $G_{ps}(a) < \Gamma_f$. In this case, the channel crack will not propagate since the energy release rate for the channel crack, G_{ss}, at indentation depth $\delta_i/t_f < 1$ is not high enough as illustrated in Fig. 17 by the point where the energy release rate for the plane strain crack, G_{ps}, and the energy release rate for the channel crack, G_{ss}, at indentation depth $\delta_i/t_f < 1$ intersects. Since the fracture toughness is estimated based on the channel crack, longer initial defects will not influence the accuracy of the method.

In the case where the length of the initial defects are shorter than those required, the defects will not initiate at the indentation depth $\delta_i/t_f = 1$ since the energy release rate for the plane strain crack, G_{ps}, is lower than the fracture toughness, Γ_f, i.e. $G_{ps}(a < a_{init}) < \Gamma_f$ at indentation depth $\delta_i/t_f = 1$. If no plane strain crack is present channeling cannot occur and fracture toughness cannot be estimated. With deeper indentation $\delta_i/t_f > 1$, the energy release rate for the plane strain crack, G_{ps}, will increase and the plane strain crack will propagate as illustrated in Fig. 17 by the point where the energy release rate for a plane strain crack, G_{ps}, at indentation depth $\delta_i/t_f > 1$ intersects the curve for fracture toughness, Γ_f. The plane strain crack will then propagate until the energy release rate for the channel crack, G_{ss}, is higher than the energy release rate for the plane strain crack, G_{ps}, illustrated in Fig. 17 by the point where the energy release rate for a plane strain crack, G_{ps}, intersects the energy release rate for channel crack, G_{ss}, at indentation depth $\delta_i/t_f > 1$. Since this point is located higher than the fracture toughness, Γ_f, this will introduce an error in the estimated fracture toughness, Γ_{dev}, i.e. the fracture toughness will be overestimated with this method. In Fig. 18, the relative error, Γ_{dev}/Γ_f, is plotted against the indentation depth, δ_i/t_f, for various deviations of the length of initial defects, a_{dev}/a_{init}.

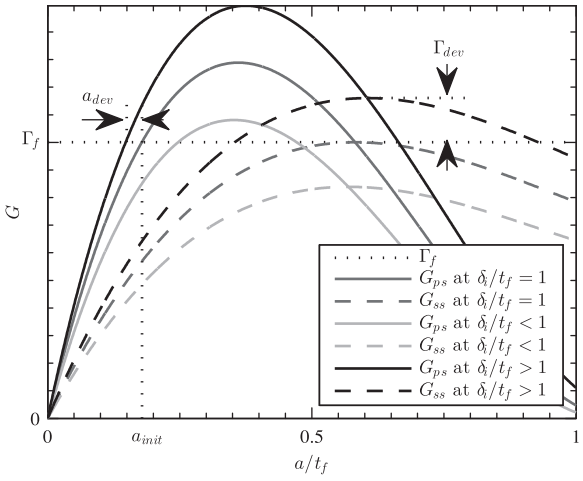

Fig. 17. Illustration of energy release rate as a function of crack depth for various indentation depths and error involved with insufficient initial flaw.

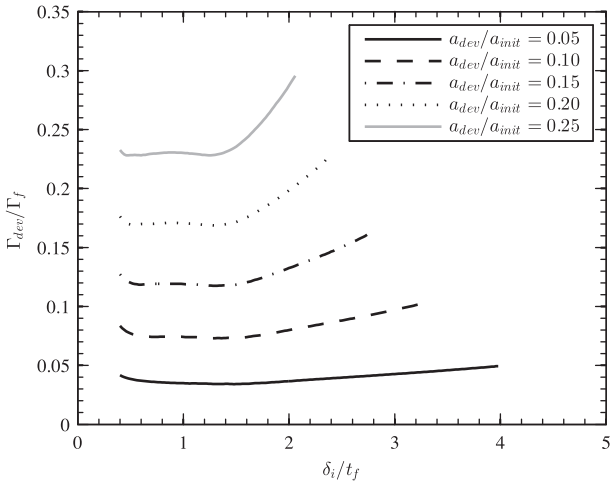

Fig. 18. Error in the estimated fracture toughness induced due to insufficient length of the initial defects.

The figure shows that the relative error in fracture toughness, Γ_{dev}/Γ_f, is rather constant for $\delta_i/t_f < 2$ and increases with δ_i/t_f for $\delta_i/t_f > 2$. For $\delta_i/t_f < 2$, the error approximately scales with a_{dev}/a_{init}. In this part, the relative error in fracture toughness, Γ_{dev}/Γ_f, roughly scales with the relative error in the size of the initial defects, a_{dev}/a_{init}. Due to convergence of the radial stress, σ_{rr}, at a certain indentation depth, δ_i, the energy release rate for the plane strain crack, G_{ps}, stops increasing. Thus, if the length of the initial defects are smaller than the length calculated, a_{init}, the plane strain crack can not propagate. As a result, the curves in Fig. 18 terminates.

Thus, it is important that the length of the initial defects are of equal length or longer than the estimated length of the initial defects in order not to overestimate the fracture toughness. In Fig. 19 the minimal length of the initial defects for the method to be accurate, a_{init}, is plotted versus the indentation depth, δ_i/t_f.

12. Experiments

Alumina films (Al_2O_3) were synthesized by reactive pulsed DC magnetron sputtering in an industrial-scale deposition unit (CemeCon CC800/9 SinOx). The temperature in the chamber during the deposition was approximately 530 °C. A bipolar MF bias of 30 V

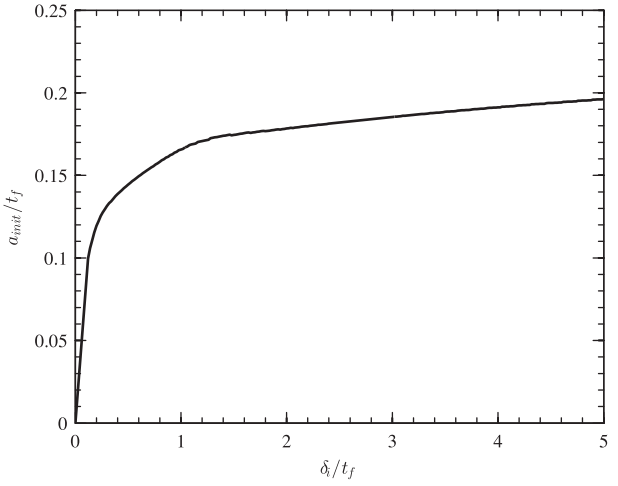

Fig. 19. Minimal length of the initial defect for the estimation of fracture toughness to be accurate.

(350 kHz) with a reverse time of 500 ns (82.5% duty cycle) was applied to the substrate. Thin TiAlN adhesion layers were deposited under the alumina films, which were deposited on Si (100) and electro-polished 316 l stainless steel substrates simultaneously. Further experimental details is given in Madsen et al. (2013). The alumina film thickness was 1.0 μm with an additional 0.2 μm TiAlN adhesion layer. In the numerical model, it was chosen to include the thickness of the adhesion layer in the thickness of the film, t_f, in order to present the method using a more simple numerical model. This was found reasonable since the thickness of the adhesion layer is thin compared to the thickness of the film and because the Young's modulus of the film and the adhesion layer is almost identical as described later.

For characterization of the film, X-ray diffraction (XRD) and X-ray reflection (XRR) experiments were performed with a Rigaku SmartLab using CuKa radiation in the grazing incidence geometry and scanning electron microscopy (SEM) was done with a Hitachi TM-1000 and a FEI NOVA 600 SEM equipped with a low vacuum detector to avoid charging of the sample. The XRD measurements showed that the alumina film contained γ-alumina and the XRR revealed a density of 3.63 g/cm^3 which is close to the tabulated density for γ-alumina (Levin and Brandon, 1998), as seen from cross sectional SEM images of the film on the silicon wafer, it had a columnar morphology. The columnar morphology may give rise to a small deviation between the numerical simulation and the experiments since the film is assumed isotropic in the numerical model.

The mechanical properties were measured by nanoindentation using a TriboIndenter (Hysitron Inc.) equipped with a Berkovich tip. In the load range 1000 μN → 9500 μN 100 indents were made. In order to avoid any substrate contribution, data was cut off at a penetration depth corresponding to approximately 10% of the film thickness t_f. The hardness, H, and the reduced elastic modulus, E_r, were determined according to the procedure by Oliver and Pharr (1992). The hardness and the Young's modulus of the alumina film were determined to 20.2 GPa and 237 GPa, respectively. The adhesion layer hardness and modulus had values of 15.3 GPa and 227 GPa, respectively. The residual stress in the film is estimated from wafer curvature measurements on silicon wafers to be approximately 0.5 GPa in tensile radial stress, σ_{rr} (Janssen et al., 2009). Residual stresses are neglected in the numerical model in these preliminary studies but the influence of residual stresses on this method is a subject for further investigations.

For fracture studies high load nano-indentations were performed with a MultiRange NanoProbe (MRN) equipped with a conical indenter tip. The included angle of the tip was 70.3° and the tip rounding was 0.76 μm according to the tip manufacturer specification. The load function was load controlled with a load period of 10 s, no hold time and 10 s unloading time. The maximum load varied from 70 mN → 85 mN in steps of 2.5 mN. Five indentations were made at each load. The indentations were made with an inter-spacing of 200 μm. Additional indentations were made at higher loads to improve the crack-radius statistics. In Fig. 2, an example of an indentation image is shown. A clear circumferential crack is seen and the radius of the crack, r_{crack}, has in this case been measured to 3.45 μm. The fracture is placed outside the indentation impression as predicted by the model. Also, the fracture is seen to follow the column boundaries in the film. This is not surprising since the column boundaries has been shown to have a lower density than the columns (Vink et al., 1991). Also, the defects which initiate the cracks are most likely situated in the column boundaries. The average crack radius has been measured to be 3.29 ± 0.08 μm.

The critical load was determined by ex-situ imaging of the indentations. Each indentation image was characterized by no crack, partially cracked or fully cracked. In Fig. 20, the number of the different types of fractures is shown as function of the applied load. From this data, the critical load for this film has been estimated to 80 ± 2.5 mN since by Fig. 20 the number of fully formed circumferential cracks exceed the number of partial cracks. However, the circumferential cracks in this film propagate over a small load range. Thus, there is not a single load which can be defined as the critical load for each indentation. This result was also reflected in the load curves which did not have any "pop-in" events. The critical load corresponds to a critical depth of 0.95 ± 0.05 μm as seen from Fig. 21. This way of determining the critical load is not required in cases where circumferential cracking is accompanied by a clear pop-in event in the indentation response.

In Fig. 21, five indentation curves and the average of the five curves are shown together with the simulated curve. There is a discrepancy between the experimental curves and the simulation which may be explained by small deviations between the numerical model and the system used for the experiments, as described earlier.

The critical depth seen from Fig. 21 is used with Fig. 14 to obtain the fracture toughness of the film, Γ_f. In this case, a value of 154 ± 10 J/m^2 is found. The stress intensity factor for the film, K_c, is calculated using Eq. (2) and is found to a value of 6.31 MPa$\sqrt{m}$. The fracture toughness for the film is found reasonable since the fracture toughness for bulk alumina is 3–5 MPa$\sqrt{m}$

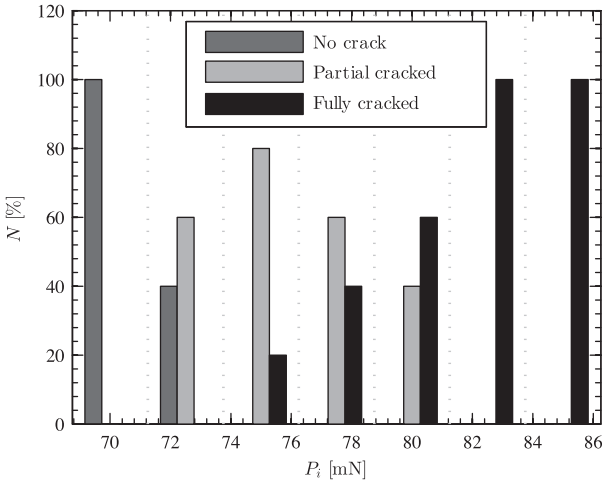

Fig. 20. Critical load statistics.

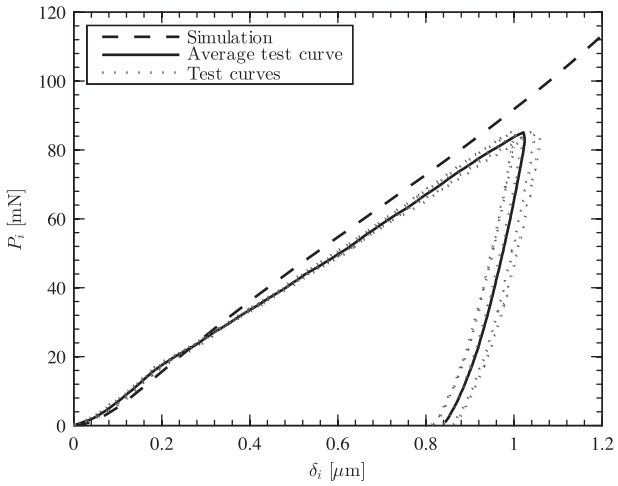

Fig. 21. Indenter response for experiments and simulation.

(Ashby and Jones, 1996). However, for the present system, information on initial flaw size has not been available, for which reason the corrections to the calculated fracture toughness in case of insufficient initial flaw size, discussed in Section 11, have not been applied.

Furthermore, the critical depth can be used to predict the crack radius, r_{crack}, and here a value of 3.20 ± 0.10 μm is obtained from Fig. 15. This compared with the measured value of 3.29 ± 0.08 μm to within the uncertainties related to the two radii.

The circumferential crack in Fig. 2 will not propagate all the way to the interface. From Fig. 16, the crack propagation will stop approximately half way through the film. At this point no experiments have verified this and it is a subject for further experiments.

From Fig. 19, the minimum length of the initial defects for the method to be precise is approximately $a_{init}/t_f = 0.16$. Thus, the fracture toughness, Γ_f, estimated for the film may be overestimated if the length of the initial defects are shorter. The size or the shape of the initial defects in the alumina film used in the experiments are not know in any details and no information about the overestimation of fracture toughness, Γ_{dev}/Γ_f, can be given for the film.

Plasticity may have been present in the film and the adhesion layer but is neglected since linear fracture-mechanics models are used to calculate the stress intensity factors, K. This may be another reason for the discrepancy between the indentation response from the experiments and the numerical simulation in Fig. 21. Also, plasticity may effect the calculation of the stress intensity factor, K, and for that reason the size of the plastic zone around the crack tip is investigated. A rough first-order estimate of the size of the plastic zone around the crack tip for a plane strain crack, r_p, is given by Anderson (2005)

$$r_p = \frac{1}{6\pi}\left(\frac{K_c}{\sigma_y}\right)^2 \tag{8}$$

where K_c is the critical stress intensity factor for the film and σ_y is the yield stress for the film which is roughly estimated as a third of the film hardness, $H/3$. In this case the yield stress is 6.7 GPa which gives a 0.04 μm plastic zone around the crack tip which is small compared to the thickness of the film, t_f, and the length of the crack, a_{crack}.

Linear elastic fracture mechanics as used in this paper is based on the concept of small scale yielding (s.s.y) i.e. the plastic zone at the crack tip is sufficiently small compared to the crack length and other relevant geometric length. Due to the calculated size of the plastic zone small scale yielding is assumed fulfilled and linear fracture mechanics are sufficient for estimating the fracture toughness for the film, Γ_f.

13. Conclusion

A method to estimate fracture toughness, Γ_f, from the first indenter-induced circumferential crack in a thin film bonded to a substrate have been suggested. Besides fracture toughness, Γ_f, the method gives informations about the depth of the circumferential crack, a_{max}, when it is channeling around the indenter, the radius of the circumferential crack, r_{crack}, and a minimum length of the initial defects, a_{init}, for the method to be precise.

The method is based on the stresses in the film calculated using a numerical model. The numerical model shows that the only stress with a significant influence on the circumferential crack is the radial stress, σ_{rr}, i.e. mode I loading. Since the method is based on a numerical model, it is of paramount importance that the model is consistent with the mechanical properties of the film, the substrate and, if necessary, the adhesion layer used in the experiments. If the numerical model is consistent with the experiment, it will result in a good match in the indenter response and consequently, a reliable determination of the fracture toughness.

The calculated radius of the circumferential crack, r_{crack}, can be used to show the consistence of the model and experiment. The calculated radius of the circumferential crack, r_{crack}, should match the measured radius.

The method for estimating the fracture toughness, Γ_f, yields that the circumferential crack does not propagate all the way through the film to the interface as assumed in other methods to estimate fracture toughness. It is shown that the maximum depth of the crack, a_{max}, is approximately half way through the film. At this time no experiments have verified this and it is a subject for future experiments but that unstable crack propagation can stop before the interface is consistent with experiments by Chai et al. (1999).

The model for estimating fracture toughness is independent of the initial defects. However, a minimal length of the initial defects, a_{init}, is required for the method not to overestimate fracture toughness and this minimal length of the initial defects is given. Also, the method gives an estimate of the error that rise in case of a shorter length of the initial defects, a_{init}.

Assumptions made throughout this paper may limit the procedure. Complexities in the microstructure of the film are ignored in this work and only homogeneous films are considered which may affect the accuracy of the fracture toughness estimated using the method. In cases of a non-homogeneous film the procedure used to estimate the fracture toughness of the film may be affected since the material properties found using nano-indentation may be insufficient and inaccurate to describe the response of the film. Also, the microstructure may alter the stress destribution in the film and the assumption of the crack propagating perpendicular to the surface may be wrong. The influence of complexities in the microstructure of the film is a subject for further studies.

The film is assumed linear elastic due to the use of linear fracture mechanic models. The finite element simulation revealed high stresses in the film and this may not be consistent with the choice of the linear elastic properties for the film. However, the size of the plastic zone around the crack tip did not indicate that plasticity in the film should be a problem for the method for estimating the fracture toughness for the film.

The method have been applied for obtain the fracture toughness for an alumina film deposited on stainless steel. The fracture toughness was estimated to 154 J/m^2 which is found to be reasonable for an alumina film. The result is verified by the radius of the circumferential crack, r_{crack}, and the match was within a few per-

cent. During the experiments only circumferential cracks initiating from the surface have been observed. Others have observed radial and circumferential cracks in the film initiating from the interface. If these cracks have been present during the experiments they have not reached the surface. In the present of such crack the method will been inaccurate since these crack will alter the stress distribution. If radial and circumferential cracks initiating before the circumferential crack that initiate from the surface can be implemented in the finite element model the procedure for estimating the fracture toughness for the film should be valid. However, this have not been investigated and it is a subject for further studies.

Acknowledgments

The authors thank Professor John W. Hutchinson, School of Engineering and Applied Sciences, Harvard University, Cambridge, MA, United States for supervision and useful discussions. Also, Professor Dr. Scient. Jørgen Bøttiger, Interdisciplinary Nanoscience Center (iNANO), Aarhus University, Ny Munkegade, Bldg. 1520, DK-8000 Aarhus C, Denmark for support during the experiments.

Vestas Wind Systems A/S, Hedeager 44, 8200 Aarhus N, Denmark is acknowledged for their financial support.

References

Oliver, W.C., Pharr, G.M., 1992. An improved technique for determining hardness and elastic modulus using load and displacement sensing indentation experiments. Journal of Material Research 7, 1564–1583.

An, L., Chan, H.M., Padture, N.P., Lawn, B.R., 1996. Damage-resistant alumina-based layer composites. Journal of Material Research 11 (1), 204–210.

Chai, H., Lawn, B., Wuttiphan, S., 1999. Fracture modes in brittle coatings with large interlayer modulus mismatch. Journal of Materials Research 14 (9), 3805–3817.

Chai, H., Lawn, B.R., 2004. Fracture mode transitions in brittle coatings on compliant substrates as a function of thickness. Journal of Materials Research 19 (6), 1752–1761.

Fischer-Cripps, A.C., Lawn, B., Pajares, A., Wei, L., 1996. Stress analysis of elastic–plastic contact damage in ceramic coatings on metal substrates. Journal of the American Ceramic Society 79 (10), 2619–2625.

Lardner, T.J., Ritter, J.E., Zhu, G.Q., 1997. Spherical indentation and fracture of glass plates. Journal of the American Ceramic Society 80 (7), 1851–1862.

Lee, K.S., Wuttiphan, S., Hu, X.Z., Lee, S.K., Lawn, B.R., 1998a. Contact-induced transverse fracture in brittle layers on soft substrates: a study on silicon nitride bilayers. Journal of the American Ceramic Society 81 (3), 571–580.

Lee, K.S., Lee, S.K., Lawn, B.R., 1998b. Contact damage and strength degradation in brittle/quasi-plastic silicon nitride bilayers. Journal of the American Ceramic Society 81 (9), 2394–2404.

Lawn, B.R., Lee, K.S., Chai, H., Pajares, A., Kim, D.K., Wuttiphan, S., Peterson, I.M., Hu, X., 2000. Damage-resistant brittle coatings. Advanced Engineering Materials 2 (11), 745–748.

Miranda, P., Pajares, A., Guiberteau, F., Cumbrera, F.L., Lawn, B.R., 2001. Contact fracture of brittle bilayer coatings on soft substrates. Journal of Materials Research 16 (1), 115–126.

Pajares, A., Wei, L., Lawn, B.R., Padture, N.P., Berndt, C.C., 1996. Mechanical characterization of plasma sprayed ceramic coatings on metal substrates by contact testing. Material Science and Engineering A208, 158–165.

Swain, M.V., Mencik, J., 1994. Mechanical property characterization of thin films using spherical tipped indenters. Thin Solid Films 253, 204–211.

Wuttiphan, S., Lawn, B.R., Padture, N.P., 1996. Crack suppression in strongly bonded homogeneous/heterogeneous laminates: a study on glass/glass-ceramic bilayers. Journal of the American Ceramic Society 79 (3), 634–640.

Hainsworth, S.V., McGurk, M.R., Page, T.F., 1998. The effect of coating cracking on the indentation response of thin hard-coated systems. Surface and Coatings Technology 102, 97–107.

Whitehead, A.J., Page, T.F., 1992. Nanoindentation studies of thin film coated system. Thin Solid Films 220, 277–283.

Weppelmann, E., Swain, M.V., 1996. Investigation of stresses and stress intensity factors responsible for fracture of thin protective films during ultra-micro indentation tests with spherical indenters. Thin Solid Films 286, 111–121.

Abdul-Baqi, A., der Giessen, E.V., 2002. Numerical analysis of indentation-induced cracking of brittle coatings on ductile substrates. International Journal of Solids and Structures 39, 1427–1442.

Bhattacharya, A.K., Nix, W.D., 1988. Analysis of elastic and plastic deformation associated with indentation testing of thin films on substrates. International Journal of Solids and Structures 24 (12), 1287–1298.

Pachler, T., Souza, R.M., Tschiptschin, A.P., 2007. Finite element analysis of peak stresses developed during indentation of ceramic coated steels. Surface and Coatings Technology 202, 1098–1102.

Sriram, K., Narasimhan, R., Biswas, S.K., 2003. A numerical fracture analysis of indentation into thin hard films on soft substrates. Engineering Fracture Mechanics 70, 1323–1338.

Vanimisetti, S.K., Narasimhan, R., 2006. A numerical analysis of spherical indentation response of thin hard films on soft substrates. International Journal of Solids and Structures 43, 6180–6193.

Vanimisetti, S.K., Narasimhan, R., 2007. A numerical analysis of flexure induced cylindrical cracks during indentation of thin hard films on soft substrates. Thin Solid Films 515, 3277–3282.

Zhang, S., Zhang, X., 2012. Toughness evaluation of hard coatings and thin fils. Thin Solid Films 520, 2375–2389.

Li, X., Diao, B., Bhushan, B., 1997. Fracture mechanisms of thin amorphous carbon films in nanoindentation. Acta Materialia 45 (11).

Li, X., Bhushan, B., 1998. Measurement of fracture toughness of ultra-thin amorphous carbon films. Thin Solid Film 315, 214–221.

Toonder, J.D., Malzbender, J., With, G.D., Balkenende, R., 2002. Fracture toughness and adhesion energy of sol-gel coatings on glass. Journal of Material Research 17 (1), 224–233.

Michel, M.D., Muhlen, L.V., Achete, C.A., Lepienski, C.M., 2006. Fracture toughness, hardness and elastic modulus of hydrogenated amorphous carbon films deposited by chemical vapor deposition. Thin Solid Films 496, 481–488.

Chen, J., Bull, S.J., 2009. Modelling the limits of coating toughness in brittle coated systems. Thin Solid Films 517, 2945–2952.

Cheng, Y., Li, Z., Cheng, C., 2002. Scaling relationship for indentation measurements. Philosophical Magazine A 82 (10), 1821–1829.

Wang, J.S., Sugimura, Y., Evans, A.G., Tredway, W.K., 1998. The mechanical performance of DLC films on steel substrates. Thin Solid Films 325, 163–174.

Doege, E., Meyer-Nolkemper, H., Saeed, I., 1986. Fliesskurvenatlas metallischer Werkstoffe. Hanser Verlag, München.

Timoshenko, S., Woinowsky-Krieger, S., 1959. Theory of Plates and Shells. McGraw-Hill, New York.

Steffensen, S., Jensen, H.M., 2013. Energy release rate for circular crack due to indentation in a brittle film on a ductile substrate (in press).

Tada, H., Paris, P.C., Irwin, G.R., 2000. The Stress Analysis of Cracks Handbook, third ed. Professional Engineering Publishing.

Hutchinson, J.W., Suo, Z., 1991. Mixed mode cracking in layered materials. Advances in Applied Mechanics 29, 63–191.

Beuth, J.L., 1992. Cracking of thin bonded films in residual tension. International Journal of Solids and Structures 29 (13), 1657–1675.

Madsen, N.D., Louring, S., Berthelsen, A.N., Christensen, B.H., Almtoft, K.P., Nielsen, L.P., Bttiger, J., 2013. The influence of deposition rate and target oxidation on structure and hardness of magnetron sputtered alumina coatings (in press).

Levin, I., Brandon, D., 1998. Metastable alumina polymorphs: crystal structures and transition sequences. Journal of the American Ceramic Society 81 (8), 1995–2012.

Janssen, G., Abdalla, M., Vankeulen, F., Pujada, B., Vanvenrooy, B., 2009. Celebrating the 100th anniversary of the Stoney equation for film stress: developments from polycrystalline steel strips to single crystal silicon wafers. Thin Solid Films 517, 1858–1867.

Vink, T.J., Somers, M.A.J., Daams, J.L.C., Dirks, A.G., 1991. Stress, strain, and microstructure of sputter-deposited Mo thin films. Journal of Applied Physics 70 (8).

Ashby, M.F., Jones, D.R.H., 1996, . Engineering Materials, second ed., vol. 1. Butterworth Heinemann.

Anderson, T.L., 2005. Fracture Mechanics, third ed. Taylor and Francis Group.